[40] Mitchell, J. K., "Current Lunar Soil Research," *Journal of the Soil Mechanics and Foundations Division, ASCE*, Vol. 90, May 1964, pp. 53–83.

[41] Waters, R. H., "The Effect of Porosity on Shearing Resistance and Thermal Conductivity for Amorphous Soils in Vacuum," Ph.D. thesis, Jan. 1967, Texas A & M, College Station, Texas.

[42] Ryan, J. A. and Baker, M. B., "Adhesional Behavior of Air and Ultrahigh Vacuum Formed Silicate Surfaces in Relation to the Moon," *Adhesion or Cold Welding of Materials in Space Environments*, STP 431, 1967, American Society for Testing Materials, Philadelphia, Pa., pp. 234–247.

[43] Bowden, F. P., "The Nature and Topography of Solid Surfaces and the Study of Van der Waals Forces in Their Immediate Vicinity," *Fundamentals of Gas-Surface Interactions*, edited by H. Saltsburg, J. Smith, and M. Rogers, Academic Press, New York, 1967.

[44] Vey, E. and Nelson, J. D., "Relative Cleanliness as a Measure of Lunar Soil Strength," *Journal of Geophysical Research*, Vol. 73, No. 12, June 1968, pp. 3747–3764.

[45] Lee, D. G., "The Compressibility of a Simulated Lunar Soil in Air and in Ultrahigh Vacuum," M.S. thesis, 1969, Air Force Institute of Technology, Wright-Patterson Air Force Base, Ohio.

[46] Fogelson, D. E., "Simulated Lunar Rocks," *Proceedings of the Working Group on Extraterrestrial Resources*, SP-177, NASA, Washington, D.C., 1968.

[47] Green, J., "Selection of Rock Standards for Lunar Research," *Annals of the New York Academy of Sciences*, Vol. 123, July 1965, pp. 1123–1147.

[48] Turkevich, A. L., Patterson, J. H., and Franzgrote, E. J., "The Chemical Analysis of the Lunar Surface," *American Scientist*, Vol. 56, No. 4, Winter 1968, pp. 312–343.

[49] Leonards, G. A. and Girault, P., "A Study of the One-Dimensional Consolidation Test," *Proceedings of the 5th International Conference on Soil Mechanics*, International Society of Soil Mechanics and Foundation Engineering, Vol. 1, 1961, pp. 123–127.

[50] Hendron, A. J., "The Behavior of Sand in One-Dimensional Compression," Ph.D. thesis, 1963, Univ. of Illinois, Urbana, Illinois.

[51] Gilboy, G., "The Compressibility of Sand-Mica Mixtures," *Proceedings of the American Society of Civil Engineers*, Vol. 54, 1928, pp. 555–568.

[52] "Preliminary Foundation Concepts for a Lunar Astronomical Observatory," GSF-69 Design Study, June 1969, Air Force Institute of Technology, Wright-Patterson Air Force Base, Ohio.

NOVEMBER 1970 J. SPACECRAFT VOL. 7, NO. 11

Revised Lunar Surface Thermal Characteristics Obtained from the Surveyor V Spacecraft

L. D. Stimpson* and J. W. Lucas†
Jet Propulsion Laboratory, Pasadena, Calif.

Higher lunar surface temperatures have been obtained from Surveyor data than from Earth-based telescope measurements. In addition, temperatures derived from different sensors located on the Surveyor spacecraft were not entirely compatible. This paper presents the results of error analyses on the Surveyor V thermal data. In the compartments, heat conducted from the other faces is significant and is included in the latest calculations. Derived postsunset temperatures from solar panel data have total errors similar to those from the compartment thermal-sensor data. The actual temperature-sensor measurement inaccuracies, uncertainties in view factors, and conduction effects are the most significant sources of error. Other sources are uncertainties in internal heat loss, solar absorptance, and emissivity. Error bands for these factors are described. The overlapping of these error bands with each other and with the Earth-based results illustrates the degree of agreement of the data from the different sources. For postsunset, Surveyor V data previously had inferred a thermal parameter (γ), of about 400, whereas Earth-based measurements indicated $\gamma \simeq 850$. The latest compartment-based γ from Surveyor V is near 600 and from solar panel data it is near 1000.

Nomenclature

C = mc_p/A = heat capacity coefficient, w-hr/°K-m²
F_{ij} = view factor from surface i to surface j
K = kA_c/LA_i = conductivity coefficient, w/°K-m²
$\dot{q}$ = conduction heat flux from inside of the compartment to the outboard face = 3.5 w/m²
S = solar radiation = 1375 w/m²
T = temperature, °K
α_s = solar absorptance
$\alpha',\beta',\gamma',\delta'$ = orientation angles
β = angle between direction of sun and normal to panel
γ = $(k\rho c)^{-1/2}$, cm² sec$^{1/2}$ °K/gm-cal
ϵ = emittance
σ = Stefan-Boltzmann constant = 5.675×10^{-8} w/m²-°K
ρ_1 = lunar albedo, lunar reflectance to solar irradiation = 0.077 (Earth-based)
ϕ = sun elevation angle above lunar horizon, deg

Subscripts

0 = compartment surface containing thermal sensor (inorganic white); α_{0s} = 0.20, ϵ_0 = 0.87
1 = sunlit lunar surface; ϵ_1 = 1 (brightness assumption)
1′ = shaded lunar surface
2,3 = vertical sides of compartment (inorganic white)
4 = inboard surface (polished aluminum); α_{4s} = 0.10, ϵ_4 = 0.04
5 = bottom (polished aluminum)

Presented as Paper 69-594 at the AIAA 4th Thermophysics Conference, San Francisco, Calif., June 16–18, 1969; submitted January 22, 1970; revision received August 12, 1970. This paper presents the results of one phase of research carried out at the Jet Propulsion Laboratory, California Institute of Technology, under Contract NAS 7-100, sponsored by NASA.

* Member of the Technical Staff. Member AIAA.
† Manager for Research and Planetary Quarantine. Associate Fellow AIAA.

6 = top (inorganic white; exclusive of thermally isolated mirrors)
6′ = compartment mirror surfaces; $\epsilon_{6'} = 0.79$
7 = sunlit solar panel sides; $\epsilon_7 = 0.8$ (solar cells)
7′ = shaded solar panel sides; $\epsilon_{7'} = 0.84$ (organic white)
8 = planar array antenna; $\epsilon_8 = 0.88$ (black)
9 = solar stepping motor; $\epsilon_9 = 0.86$ (organic white, 3M)

Introduction

OF the five Surveyor spacecraft that landed on the lunar surface, Surveyor V (Fig. 1) was of most interest from a thermophysical standpoint. Surveyor V landed inside a small crater (Fig. 2). It transmitted data during the first lunar day, for five Earth days into the first night, during the second lunar day starting shortly before noon, and for nine Earth days into the second lunar night. The spacecraft had a different tilt orientation during each of these periods as a result of two-leg shock absorbers compressing at the first sunset, recovering partially on the second lunar day, and then with only one leg compressing during the second sunset. Also, an eclipse of the Surveyor V site occurred during the second lunar day.

Surveyor V had 75 thermal sensors located primarily internal to the spacecraft to monitor the performance of its subsystems. There was no science instrumentation specifically for measurement of the lunar surface temperature. Fortunately, there were several thermal sensors located on panels which viewed the lunar surface. The solar panel and planar-array antenna each had a thermal sensor, two other sensors were on the upper part of the mast, and there was one each on electronic compartments A and B. The compartments were insulated outside with multilayer superinsulation. Heat was rejected during the hot lunar day through bimetal-actuated (semiactive) thermal switches connected to highly polished Vycor mirrors on the top of each compartment. At sunset the thermal switches opened to isolate the interior from the exterior. Internal electrical heaters were available to warm the compartments.

Surveyor V landed in a small 9 × 12 m crater in the Sea of Tranquility (Fig. 2). The spacecraft was on a considerable slope with leg 1 on the upper rim of the crater. The compartments were tilted back and were above the local plane; thus the outboard faces also viewed over the edge of the small crater, with compartment A viewing southeast and compartment B viewing west. On each compartment, a temperature sensor was located on the inside surface of the outer aluminum cover. Early determinations of the lunar surface temperature assumed a model in which this outer aluminum cover was essentially isolated from the rest of the compartment except for a small heat loss from inside. Later efforts described herein take into account a small but significant heat flow from the other aluminum side covers.

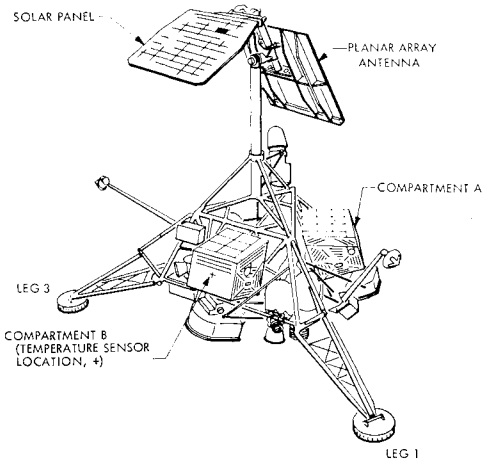

Fig. 1 Surveyor spacecraft configuration.

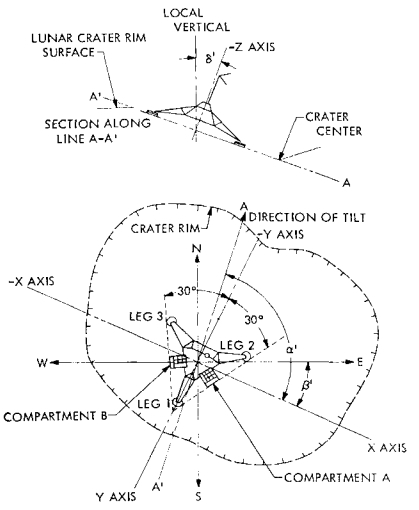

Fig. 2 Surveyor V landed orientation.

It would not be too surprising to find discrepancies between Surveyor and Earth-based measurements because of the great difference in sample sizes—Earth-based resolution is ~18 km. Some of the discrepancies found among the compartment, solar panel, and Earth-based lunar surface temperatures from earlier work[1–3] are highlighted in Fig. 3. During the morning, the lunar surface temperature derived from compartment B was higher than from Lambertian theory. The peak could be explained by the presence of directional thermal emission from the lunar surface. The compartment was viewing west and would expect to detect a greater thermal emission from the lunar surface with the morning sun over its "shoulder." The agreement with Lambertian theory during the afternoon was good.

After sunset the lunar soil cooling behavior is dependent upon the lunar soil characteristics. This is represented theoretically by the two different γ curves shown in Fig. 3; $\gamma = (k\rho c)^{-1/2}$ serves as a convenient thermophysical reference for soil. The early results from Surveyor V compartment data suggested a γ of about 400, whereas some preliminary results derived from solar panel data suggested a value greater than 800. Further confusion has existed because the Earth-based postsunset measurements indicated a γ of ~850, whereas the Earth-based eclipse measurements indicated ~1370.

The largest discrepancy between Surveyor and Earth-based temperature measurements is from eclipse measurements, which will be reported later. The lunar surface temperatures obtained from the Surveyor V compartment data during an eclipse on the second lunar day were about 100°F higher than those from Earth-based eclipse measurements. A preliminary check using solar panel data resulted in lunar surface tempera-

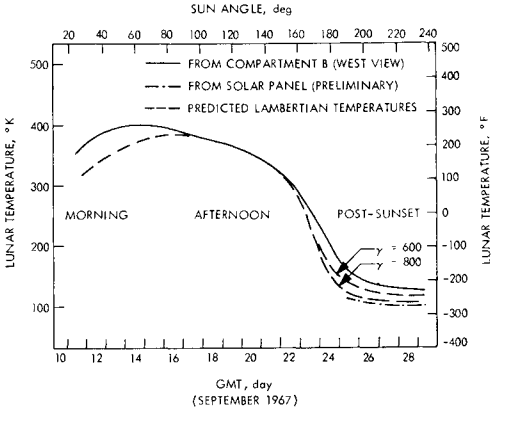

Fig. 3 Preliminary lunar surface temperature from Surveyor V compartment B and solar panel data.

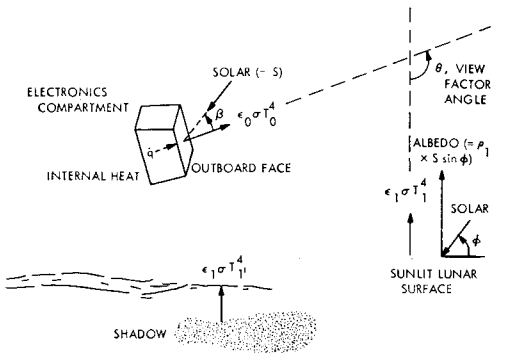

Fig. 4 Heat balance for compartment.

tures nearer the Earth-based values. The same peculiar trend occurred on Surveyor III, which had experienced an eclipse on the first lunar day. In this paper, we only analyzed Surveyor V daytime and postsunset data, and obtained an improved correlation.

Analytical Techniques

Earlier calculations[1–3] of the lunar surface temperatures from Surveyor V compartment thermal sensor data were based upon the simplified radiation heat-balance equation depicted in Fig. 4. An outboard compartment face was assumed to be thermally isolated from the remainder of the spacecraft except for a small conductive heat loss $\dot{q}$ from the interior of a compartment.

The error analyses (discussed below) indicated that a significant amount of heat also was conducted from the other faces of the compartment. The calculations in this paper have included this effect.

Equation (1) is a representation heat-balance equation for a compartment face and in particular for the outboard face that contains the thermal sensor. The terms in Eq. (1) in sequence from left to right are as follows. The energy radiated by the outboard compartment face is equal to nine energy inputs: infrared (IR) radiation from the sunlit lunar surface, IR from the shaded lunar surface, direct solar radiation, indirect solar radiation (albedo) from the lunar surface, heat flux from inside the compartment, and heat conducted from the other faces of the compartment (the last four terms);

$$\epsilon_0\sigma T_0^4 = \epsilon_0\epsilon_1 F_{01}\sigma T_1^4 + \epsilon_0\epsilon_1 F_{01'}\sigma T_{1'}^4 + \alpha_{0_\phi} S\,(\cos\beta + \rho_1 F_{01}\sin\phi) + \dot{q} + K_{20}(T_2 - T_0) + K_{30}(T_3 - T_0) + K_{50}(T_5 - T_0) + K_{60}(T_6 - T_0) \quad (1)$$

The equations for the remaining five sides are similar in form to Eq. (1).

An assumed value of 200°K (−100°F) was used for the shaded lunar surface. This assumed value is adequate, since the shadow heat input term was only of minor significance due to small view factor values involved, and then only during a small part of the lunar day. An approximate value of 3.5 w/m², found from cold chamber tests, is used for the heat flux $\dot{q}$ from the inside. This heat conduction term was important after sunset and during the totality of the eclipse.

A predominantly radiative heat-balance equation was used for determining the lunar surface temperature from Surveyor solar panel thermal sensor data depicted in Fig. 5. The thermal sensor was centrally located on the underside of the panel. Both sides of the solar panel emitted heat and also viewed the lunar surface, space, and other spacecraft components. Those components of primary influence were the planar array, the mast and the mirror surfaces on top of the compartments. Also included was the heat conduction through the mast. The heat flux density balance equation for the solar panel is

$$(\epsilon_7 + \epsilon_{7'})\sigma T_7^4 = (\epsilon_7 F_{71} + \epsilon_{7'} F_{7'1})\epsilon_1\sigma T_1^4 + (\epsilon_7 F_{78} + \epsilon_{7'} F_{7'8})\epsilon_8\sigma T_8^4 + \epsilon_{7'}\epsilon_{6'} F_{7'6'} T_{6'}^4 + K_{97}(T_9 - T_7) - C\dot{T}_7 \quad (2)$$

A similar equation exists for the planar-array antenna.

Certain coordinate transformations were required to determine the view factors and sun angles for each of the compartment faces, the solar panel, and the planar-array antenna. Each view factor required a vectorial description of the normal to the face or panel and to the local lunar surface. In the simplest case, the view factor was obtained (see Fig. 4) by the equation

$$F_{ij} = \tfrac{1}{2}(1 + \cos\theta) \quad (3)$$

To find the angle θ, the local lunar surface slope and the tilt of the face or panel from the local horizon were required. The cosine of the sun angle on a face was the scalar (dot) product of the normal vector and the sun vector, which varied with the lunar day.

It was easier to express the vectors for the face normals first in terms of spacecraft coordinates (Fig. 2). The normals to the compartment A faces (r_i) are outboard: $\mathbf{r}_0 = 0.813\mathbf{i}_{SC} + 0.470\mathbf{j}_{SC} - 0.342\mathbf{k}_{SC}$; side: $\mathbf{r}_2 = 0.500\mathbf{i}_{SC} - 0.866\mathbf{j}_{SC} = -\mathbf{r}_3$; inboard: $\mathbf{r}_4 = -\mathbf{r}_0$; bottom: $\mathbf{r}_5 = 0.295\mathbf{i}_{SC} + 0.171\mathbf{j}_{SC} + 0.940\mathbf{k}_{SC}$; and top: $\mathbf{r}_6 = -\mathbf{k}_{SC}$.

The normals to the compartment B faces are identical except that the signs are reversed on the first term of $\mathbf{r}_0$, the second term of $\mathbf{r}_2$, and the first term of $\mathbf{r}_5$.

The normal to the sunlit side of the solar panel was expressed in terms of four angles which were the solar (θ_S), polar (θ_P), elevation (θ_E), and roll (θ_R) angles shown in Fig. 6. The solar panel normal in spacecraft coordinates is

$$\mathbf{r}_7 = [\cos(\theta_S + \theta_P)\cos\theta_R - \sin(\theta_S + \theta_P)\sin\theta_E \sin\theta_R]\mathbf{i}_{SC} + [\cos(\theta_S + \theta_P)\sin\theta_R + \sin(\theta_S + \theta_P)\sin\theta_E \cos\theta_R]\mathbf{j}_{SC} + [\sin(\theta_S + \theta_P)\cos\theta_E]\mathbf{k}_{SC} \quad (4)$$

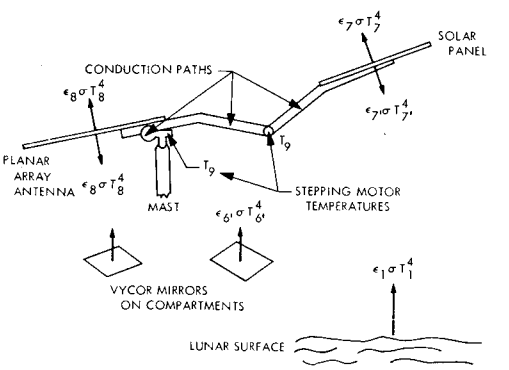

Fig. 5 Heat balance for solar panel.

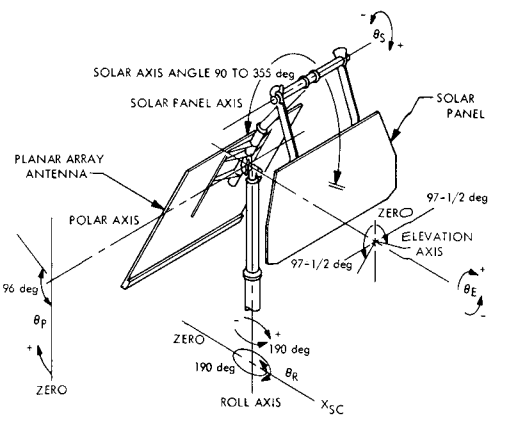

Fig. 6 Solar panel coordinate system.

Table 1 Surveyor V local lunar horizon orientation

	α', deg	β', deg	γ', deg	δ', deg
First day	97.6	−24.5	−16.9	19.5
First night	101	−25	−14	24.5
Second day	103.8	−25.4	−11.6	19.2
Second night	100.2	−25.6	−15.4	21.8

The coordinate transformation required to change the previous vectors into local coordinates (**i**,**j**,**k**) corresponding to east, north, and local zenith is

$$a = (a_{SC}\sin\alpha' + b_{SC}\cos\alpha')\cos\gamma' + [(-a_{SC}\cos\alpha' + b_{SC}\sin\alpha')\cos\delta' + c_{SC}\sin\delta']\sin\gamma' \quad (5a)$$

$$b = (a_{SC}\sin\alpha' + b_{SC}\cos\alpha')\sin\gamma' - [(-a_{SC}\cos\alpha' + b_{SC}\sin\alpha')\cos\delta' + c_{SC}\sin\delta']\cos\gamma' \quad (5b)$$

$$c = (-a_{SC}\cos\alpha' + b_{SC}\sin\alpha')\sin\delta' - c_{SC}\cos\delta' \quad (5c)$$

where (a_{SC}, b_{SC}, c_{SC}) and (a,b,c) are coefficients of the face normal vectors expressed alternatively as, for example

$$\mathbf{r}_i = a_{SC}\mathbf{i}_{SC} + b_{SC}\mathbf{j}_{SC} + c_{SC}\mathbf{k}_{SC} = a\mathbf{i} + b\mathbf{j} + c\mathbf{k} \quad (6)$$

and the spacecraft orientation angles α', β', and δ' are shown in Fig. 2; and

$$\gamma' = \alpha' + \beta' - 90 \quad (7)$$

Surveyor V had four known different orientations with respect to the local lunar horizon; first lunar day, first lunar night after two legs compressed, second lunar day when they nearly recovered, and second lunar night after one leg compressed. These different orientations‡ were as shown in Table 1.

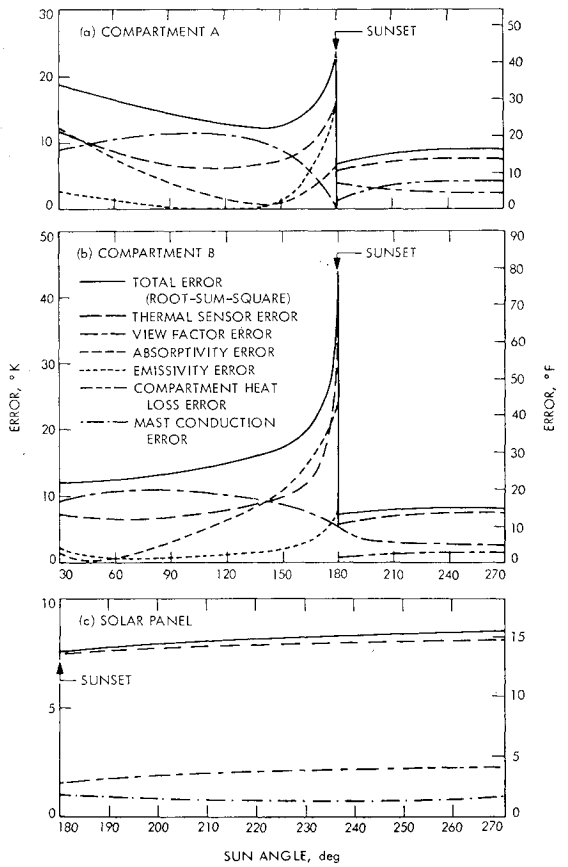

Fig. 7 Errors from Surveyor V: a) compartment A; b) compartment B; c) solar panel data after sunset.

A JPL steady-state thermal analyzer program, TAS-1B, was used to determine the lunar day and postsunset results from both compartment and solar panel thermal-sensor data. This is a relaxation program that computes the heat flow at each node except where specified as constant, and includes conductive, and radiosity (interreflection) effects. The lunar surface, solar flux, and space normally dominate the situation compared with the relatively small spacecraft. Telemetered thermal-sensor data from the spacecraft were used as radiometric measures of the lunar surface temperature. The manner in which this was accomplished on the computer was to assume different values of lunar surface temperature at selected time points and to calculate the sensor measurements that would have been obtained. By comparison with the actual telemetered data at these same time points, convergence to the appropriate lunar surface temperature was achieved.

A North American Aviation computer program, CONFAC II, was used to obtain the view factors F_{ij}. The coordinate transformations described previously were readily solved by using a Tymshare computer.

Error Analyses

Error analyses were performed on the Surveyor-based data because of the discrepancies found among the results obtained from compartment, solar panel, and Earth-based measurements. In the first error analysis, Eq. (1) was investigated analytically for errors contributing to the uncertainty of lunar surface temperature T_1. The main contributors were found to be the inaccuracy in view factor F_{01}, the uncertainty in thermally-sensed temperature T_0, and the uncertainty in internal heat loss $\dot{q}$ after sunset. Others which contributed to a lesser extent were α_{0s}, ϵ_0, S, and β. A similar analytical study of the solar panel [Eq. (2)] also showed the view factors and the telemetered temperature data to be the principal error contributors for the solar panel source.

Heat conducted around the outside of the compartments from the other faces creates an upward bias in the lunar surface temperature. This was mainly due to the two side faces that were vertical and viewed more warm lunar surface than did the outboard face which was tilted back 20°. Note also that one of the sides is almost always illuminated by the sun during the day. In some missions, either early in the morning or late in the afternoon, the sun also heated the inboard face to rather high temperatures, since it was a polished aluminum (low emissivity) surface. These effects have been included in Eq. (1).

Figure 7 shows the results obtained from a subsequent error analysis performed by using a computer. Figure 7a shows the individual contributing-error sources from compartment A data and Fig. 7b from compartment B on Surveyor V. These are reflected in subsequent figures as error bands placed about the results obtained. Note that the errors become magnified near sunset. The total errors, assumed to be independent from each other, were obtained by taking a root-sum-square of individual errors.

Error sources from the solar panel postsunset data are shown in Fig. 7c. The total error is similar to that obtained from the compartments. The temperature sensor error is the predominant source in the three figures, especially after sunset. The mast conduction error shown in Fig. 7c is primarily due to uncertainties in temperature sensor measurements on the mast.

Use of the solar panel data to predict daytime lunar surface temperatures would result in rather large errors. This is due to the higher sensitivity of the solar panel to the direct solar

‡ Data were derived during lunar operations from engineering measurements of solar panel and planar-array antenna orientations.

input (and less sensitivity to the lunar surface) and the uncertainty in temperature due to variable electrical power loading.

A good correlation exists between the error analysis results obtained from the computer and those obtained analytically from Eqs. (1) and (2). Thus, error sources previously found to have insignificant effects upon the total error have been omitted from Fig. 7.

The individually assumed errors for these analyses were

$\Delta T_i = \pm 7.2°\text{F}\ (\pm 4°\text{C})$ $\quad \Delta F_{ij} = \pm 10\%$

$\Delta \epsilon_i = \pm 0.02$ for painted surfaces,

$+0.02, -0.01$ for polished aluminum

$\Delta \alpha_i = \pm 0.02$ $\quad \Delta \dot{q} = \pm 20\%$ $\quad \Delta K_{ij} = \pm 10\%$

Comparison of Results

The lunar surface daytime temperatures obtained from Surveyor V compartment data are compared in Fig. 8 with the Lambertian prediction based upon Earth measurements. Note that the revised results using Eq. (1), which included side conduction effects, compares more favorably with the Lambertian curve. There still is some evidence of directionality, particularly in Fig. 8b. Figure 2 indicated that the outboard face of compartment B viewed the west, so that a directional effect (temperature increase) would be expected during the lunar morning, which is evident. The error band in the morning for compartment B suggests rather clearly that a directional trend exists. The trend is not clear in Fig. 8a. However, compartment A viewed southeast rather than directly east or west and would not be expected to show a directionality effect in the lunar afternoon. Also indicated in Fig. 8 is that the earlier predicted directionality trend has been reduced to about one-half in intensity.

Figure 9a compares the postsunset lunar surface temperatures from the original compartment model with the original

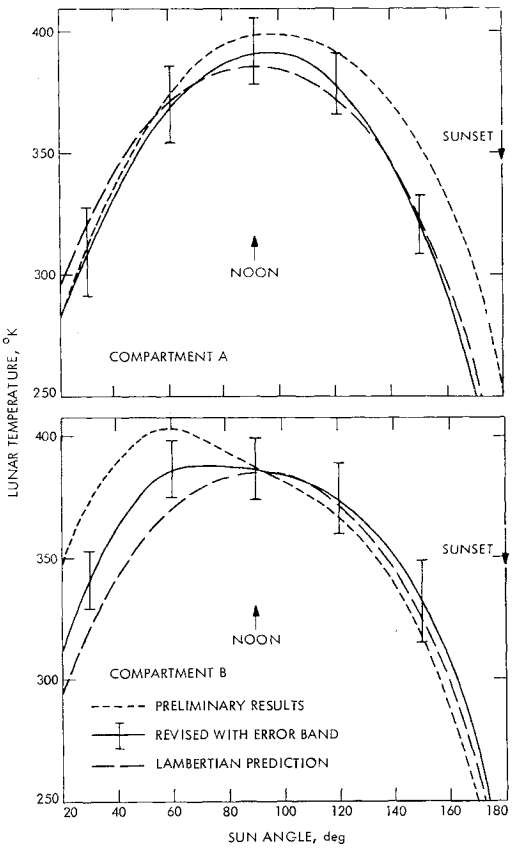

Fig. 8 Lunar surface temperatures from Surveyor V: a) compartment A; b) compartment B.

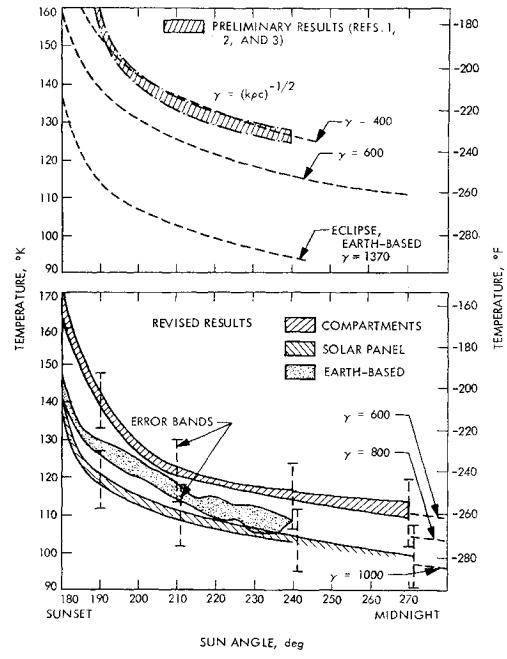

Fig. 9 Postsunset lunar surface temperatures from compartment data (top) and various sources (bottom).

Earth-based eclipse measurements, and with theoretical γ curves. In Fig. 9b the revised γ from compartment data has changed to 600. Taking the geometry changes into account for both lunar postsunset periods results in the same lunar surface temperatures, evident by the narrow band.

The γ curves assume a lunar surface having thermal characteristics that are constant. Actually, the lunar surface properties are expected to vary with depth of soil and with temperature.[4,5] Thus a difference in behavior between the constant γ curves and the compartment band is to be expected.

In Fig. 9b, the solar panel band was derived from the first and second lunar nights on Surveyor V, and it has a decreasing behavior similar to the compartment band but with $\gamma \simeq 1000$. The Earth-based postsunset measurements by Wildey, Murray, and Westphal[6] are shown for comparison, however, with an unspecified error band.

Error bands are shown in Fig. 9b for the compartment and solar panel-based results. These were presented in more detail in Fig. 7. Some over-lap between compartment and solar-panel based results is evident.

Theoretical curves are included on the right-hand side in Fig. 9b for values of γ equal to 600, 800, and 1000. Note that the compartment based trend fits a γ of about 600, the Earth-based fits an average γ of about 850, and the solar panel based trend fits a γ of about 1000.

Conclusions

The revised daytime lunar surface temperatures from Surveyor compartment data still show the presence of directionality but with about one-half the intensity previously given.

The correlation of postsunset results from compartment data with Earth-based data has been improved. The revised compartment model has resulted in lower surface temperatures. Further, the use of Earth-based postsunset, rather than eclipse data, has increased the lunar surface temperature. In addition to the revision of the compartment data, the inclusion of the solar panel results provides an average lunar surface temperature from Surveyor, which coincides with Earth-based results.

It is suggested that the difference between the compartment and solar panel temperatures is due to the compartments having viewed lunar surface nearer the spacecraft than the solar

panel. The vernier rocket exhaust upon landing may have compacted or blown the upper fluff away nearest the spacecraft.

Subsequent effort was directed toward analyzing the eclipse data, and data from the other Surveyor missions. These results are given in Ref. 7.

References

[1] Lucas, J. W. et al., "Lunar Surface Temperatures and Thermal Characteristics," *Surveyor V Mission Report, Part II: Science Results*, TR 32-1247, 1967, Jet Propulsion Lab., Pasadena, Calif.

[2] Vitkus, G., Lucas, J. W., and Saari, J. M., "Lunar Surface Thermal Characteristics During Eclipse from Surveyors III, V, and after Sunset from Surveyor V," *AIAA Progress in Astronautics and Aeronautics: Thermal Design Principles of Spacecraft and Entry Bodies*, Vol. 21, edited by G. T. Bevans, Academic Press, New York, 1969, pp. 489–505.

[3] Lucas, J. W. et al., "Lunar Surface Temperatures and Thermal Characteristics: Surveyor V Science Results," *Journal of Geophysical Research*, Vol. 73, No. 22, Nov. 15, 1968, pp. 7209–7219.

[4] Jones, B. P., "Density-Depth Model for the Lunar Outermost Layer," *Journal of Geophysical Research*, Vol. 73, No. 24, 1968, pp. 7631–7635.

[5] Winter, D. F. and Saari, J. M., "A New Thermophysical Model of the Lunar Soil," Document DI-82-0725, Boeing Scientific Research Lab., 1968.

[6] Wildey, R. L., Murray, B. C., and Westphal, J. A., "Reconnaissance of Infrared Emission from the Lunar Nighttime Surface," *Journal of Geophysical Research*, Vol. 72, No. 14, 1967, pp. 3743–3749.

[7] Stimpson, L. D. et al., "Revised Lunar Surface Temperatures and Thermal Characteristics from Surveyor," *Analysis of Surveyor Data*, TR 32-1443, 1969, Jet Propulsion Lab., Pasadena, Calif.

NOVEMBER 1970 J. SPACECRAFT VOL. 7, NO. 11

Waffle Plates with Multiple Rib Sizes: I. Stability Analysis

LAWRENCE D. HOFMEISTER*
TRW Systems, Redondo Beach, Calif.

AND

LEWIS P. FELTON†
University of California, Los Angeles, Calif.

A method is presented for the gross buckling analysis of waffle plates having multiple sizes of ribs in each stiffening direction. Rectangular plates having two distinct size ribs arranged in orthogonal and equilateral configurations are investigated in detail. General biaxial in-plane load conditions are considered. The stability criterion is developed by minimizing the total potential energy of the systems. Several examples are presented to illustrate applications of the formulations to plates with discrete ribs, closely spaced ribs, and combinations of the two. Where possible, results are compared to solutions obtained from other sources with good agreement.

Nomenclature

A,Z,I	=	geometric parameters
a,b	=	plate dimensions
c_i,e_j	=	coordinates of orthogonal stiffeners
d	=	primary rib spacing
E_s,E_1,E_2	=	moduli of elasticity of skin, primary, and secondary ribs, respectively
$\bar{e}_x,\bar{e}_y,\bar{e}_{xy}$	=	load eccentricities with respect to middle surface
$\mathbf{F}$	=	vector of generalized forces
$\mathbf{K}$	=	stiffness matrix
L	=	number of displacement functions
N_{1j}	=	critical load
N_x,N_y,N_{xy}	=	applied loads
P_i	=	distributed forces in primary ribs
$\mathbf{S}_x,\mathbf{S}_y,\mathbf{S}_{xy},\mathbf{S}_j$	=	stability matrices
U_{mn},V_{mn},W_{mn}	=	displacement amplitudes
$\mathbf{U}$	=	vector of unknown displacements
h_1,h_2	=	height of primary and secondary ribs, respectively
k_{ij}	=	constants in stress-strain relations
m,n,k	=	integers
t,t_1,t_2	=	thickness of plate skin, primary, and secondary ribs, respectively
$\bar{t}_i,\bar{t}_j$	=	equivalent thickness
u,v,w	=	displacements
Π	=	strain energy
$\alpha_j,\gamma_j,\beta_j$	=	N_x/N_{1j}, N_y/N_{1j}, and N_{xy}/N_{1j}, respectively
ϵ,σ	=	strain and stress, respectively
ν_s	=	Poisson's ratio

Subscripts

s	=	plate skin
$u_{,x},w_{,xx}$	=	$\partial u/\partial x$, $\partial^2 w/\partial x^2$, respectively, etc.

Received August 8, 1969; revision received June 22, 1970. This work was partially supported by Grant NsG-423 from NASA to the late F. R. Shanley, Professor of Engineering, University of California, Los Angeles. The authors wish to acknowledge the fact that the structural concept investigated in this paper originated with him.

* Member of the Technical Staff, formerly Postgraduate Research Engineer, University of Calif., Los Angeles, Calif.

† Assistant Professor of Engineering. Member AIAA.

Introduction

IN a previous paper[1] the behavior and design of integrally stiffened waffle plates having two distinct sizes of orthogonal ribs (see Fig. 1) were investigated for the case of uni-